Static and Dynamic Axial Response of Drilled Piers. I: Field Tests

Gang Wang, M.ASCE[1]; Gyimah Kasali, M.ASCE[2]; and Nicholas Sitar, M.ASCE[3]

Abstract: A prototype pier load test program was performed to study the load-deformation and energy-dissipation characteristics of the response of drilled piers under static and dynamic axial loads. The field tests consisted of six fully instrumented drilled concrete piers 61–76 cm (24–30 in.) in diameter and 5.8–9.1 m (19–30 ft) in length. The piers were constructed on a stiff, sandy clay site adjacent to the University of California, Berkeley campus. A dynamic Fundex pile load test (PLT) was performed on each pier, followed by a static-compression or tension test and a second PLT. The field tests revealed that the stiffness and capacity of a soil-pier system depend significantly on the loading rate. For the type of piers and soil considered in the field test, the increase in dynamic stiffness versus static stiffness is approximately 20–40% at almost all displacement levels. The ultimate dynamic capacity increases approximately 30% compared with the static case. The multiple PLTs conducted on the same drilled pier also indicated that a pier may experience up to 50% stiffness and strength degradation when subjected to full load reversal. The test program showed that the PLT is a fast, innovative method to get useful site-specific information for seismic design of the pier foundation. **DOI: 10.1061/(ASCE)GT.1943-5606.0000547.**

CE Database subject headings: Piers; Dynamic loads; Axial loads.

Author keywords: Drilled pier; Dynamic loading; Axial load; Field study.

Introduction

Performance-based earthquake design of pier foundations requires an improved understanding of dynamic soil-pier interaction. Much effort has been devoted to the study of lateral response of the pier-soil system, but very few studies have addressed the axial behavior of piles and drilled piers under dynamic loading. Although seismic loads are usually viewed as being primarily horizontal, the action on the pier has a significant vertical component when the interaction of a superstructure is involved. As schematically illustrated in Fig. 1, a vertically-propagated shear wave during an earthquake causes rocking of the superstructure, which subsequently induces a vertical up-and-down axial movement of piers. The current practice in design of the axial capacity of drilled piers is usually based on theoretical calculation of the ultimate load capacity, using data from static field and laboratory tests. Similarly, the load-deformation characteristics for drilled piers are usually defined using empirical methods primarily developed for static loading. Because the typical earthquake loading rate is approximately three orders of magnitude greater than the rate of load application in a static test, both the dynamic stiffness and the load capacity tend to be underestimated. This leads to uneconomical drilled-pier design and inaccurate modeling of the response of the superstructure. Thus, for earthquake design of pier foundations, proper consideration of dynamic effects may have important economic and safety implications (Kraft et al. 1981).

As part of an effort to develop a more efficient and effective design of drilled-pier foundations, a prototype axial load test program on drilled, cast-in-place concrete piers was performed adjacent to the campus of the University of California, Berkeley. The test program was designed to evaluate the dynamic and static stiffness and capacity of vertically loaded piers. The loading rate of the load test was designed to simulate a typical earthquake loading, making the data particularly useful for earthquake design. The piers were loaded to a wide range of mobilized strains, making it possible to evaluate the nonlinear load-deformation and energy-dissipation characteristics. The results of the load tests and their interpretation are presented in this paper. As a follow-up, the load tests on the pier-soil system were numerically simulated using a nonlinear finite-element program. The results of the numerical simulations are presented in a companion paper by Wang and Sitar (2011).

Site Conditions

The drilled-pier load test program was performed at the Underhill Parking Lot on the south side of the campus of the University of California, Berkeley. The test program was aimed at developing an efficient foundation design for the seismic retrofit and construction of new residence facilities on sites adjacent to the test site. The test site is bounded to the north by Channing Way, to the east by College Avenue, to the south by Haste Street, and to the west by a new dining/student services building and an exiting apartment building. Overall, the site is underlain by typical alluvial deposits of the Temescal formation, consisting primarily of silts and clays with occasional gravel or gravelly interbeds. Two test areas were selected for the pier load test program because of their proximity to the location of a previous geotechnical investigation conducted

[1]Assistant Professor, Dept. of Civil and Environmental Engineering, Hong Kong Univ. of Science and Technology, Clearwater Bay, Kowloon, Hong Kong (corresponding author). E-mail: gwang@ust.hk

[2]Principal Engineer, Rutherford & Chekene Consulting Engineers, 55 Second Street, Suite 600, San Francisco, CA 94105.

[3]Professor, Dept. of Civil and Environmental Engineering, Univ. of California, Berkeley, CA 94720.

Note. This manuscript was submitted on December 24, 2007; approved on April 8, 2011; published online on November 15, 2011. Discussion period open until May 1, 2012; separate discussions must be submitted for individual papers. This paper is part of the ***Journal of Geotechnical and Geoenvironmental Engineering***, Vol. 137, No. 12, December 1, 2011. ©ASCE, ISSN 1090-0241/2011/12-1133–1142/$25.00.

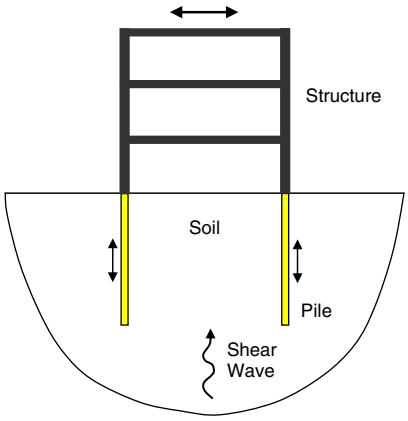

Fig. 1. Foundation-soil-structure system

in 1997. Schematic soil profiles with standard penetration test (SPT) blow counts and schematic pier layouts in the two test areas are presented in Fig. 2. The boring logs indicate that Test Area 1 [Fig. 2(a)] is underlain by a 1.8-m (6-ft)-thick layer of stiff high-plasticity clay with sand. This clay layer is underlain by a 0.6-cm (2-ft)-thick layer of medium-dense silty sand sandwiched between two thin (approximately 0.5-m-thick) sandy lean-clay layers. These upper layers are underlain by an approximately 0.9-m (3-ft)-thick layer of dense clayey sand with gravel. The clayey sand layer is underlain by hard sandy clay extending well below the zone of interest. During the 1997 field exploration, groundwater was reported to be at a depth of 6.55 m (21.5 ft). The SPT blow counts vary from 79–85 blows per meter (BPM) [24–26 blows per foot (BPF)] in the surface layers to 148–177 BPM (45–54 BPF) at depths of 6.1–7.6 m (20–25 ft).

Test Area 2 [Fig. 2(b)] is underlain by a 0.3-m (1-ft) layer of hard, sandy lean clay overlying an approximately 2.3-m (7.5-ft)-thick layer of very dense, clayey sand with gravel, which is in turn underlain by a 0.5-m (1.5-ft)-thick layer of very stiff, silty clay with sand. The silty clay layer is underlain by a sequence of dense and stiff strata, consisting of 1.1 m (3.5 ft) of dense clayey sand with gravel, 1.8 m (6 ft) of stiff sandy clay, 1.5 m (5 ft) of very stiff sandy silt, 1.1 m (3.5 ft) of dense clayey gravel with sand, and stiff sandy clay. Groundwater was encountered at a depth of 3.5 m (11.5 ft). Very high SPT blow counts [276 BPM (84 BPF)] were recorded in the upper layer, consisting of very dense clayey sand with gravel, as well as in the lower layer, consisting of dense clayey gravel with sand.

Laboratory testing on soil samples showed the degree of saturation ranges from 46% close to the ground surface to 93% at 3 m deep. Moisture contents were 22–24% for the top 3 m and 18–20% below 6 m. In Test Area 1, groundwater was encountered at a depth of 5.5 m in the middle and western pier holes. Groundwater was not encountered in any of the pier holes in Test Area 2, indicating that the groundwater level had changed since the previous site investigation in 1997.

An in situ shear-strength profile was also estimated from unconfined compression tests on soil samples from the site, as shown in Fig. 3. In general, the shear strength increases with depth, with fairly high soil strength close to the surface, indicating that part of soils may be overly consolidated because of desiccation and unloading from deep excavation during site formation. Because of the lack of direct test data on soils below 8 m, the shear-strength profile is the best estimation on the basis of our knowledge of the site conditions from many other investigations on the Berkeley campus. Spectral analysis of surface waves (SASW) measurements were also conducted along two arrays close to Test Areas 1 and 2. The shear-wave velocity profile is also plotted in Fig. 3. On the basis of the measurement, bedrock interface was interpreted to be at a depth of 13.7–18.3 m (45–60 ft), and the average shear-wave velocities in the upper 30 m (V_{s30}) were found to be 456 m/s (1496 ft/s) for Test Area 1 and 545 m/s (1788 ft/s) for Test Area 2. The plot also shows that at the depths of interest for our load tests, 6.1–9.1 m (20–30 ft), the average shear-wave velocities were estimated to be 280–310 m/s (918–1017 ft/s), corresponding to a "very dense soil and soft rock" site class according to the 1997 *Uniform Building Code*.

Load Test Program

Three drilled piers were installed in each test area, as shown schematically in Fig. 4. Each pier was given a reference name for its location and length. In Test Area 1, a 76-cm (2.5-ft)-diameter, 5.8-m (19-ft)-long pier (Pier A1-19) is flanked by two 61-cm (2-ft)-diameter, 6.1-m (20-ft)-long piers (Piers A1-20A and A1-20B), with a spacing of approximately 3.7 m (12 ft) to the middle pier. In Test Area 2, the middle pier is 61 cm (2 ft) in diameter and 9.1 m (30 ft) long (Pier A2-30), with one 61-cm (2-ft)-diameter, 6.1-m (20-ft)-long pier (Pier A2-20) installed approximately 3.7 m (12 ft) to the west, and another 61-cm (2-ft)-diameter, 7.6-m (25-ft)-long pier (Pier A2-25) approximately 3.7 m (12 ft) away to the east. For the static-compression test on piles, ASTM D1143 (ASTM 2007a, clause 3.3.1) specified "a clear distance from the test pile or pile group at least five times the maximum diameter of the largest anchor or test pile (s) but not less than 7 ft (2 m)." In Test Areas 1 and 2, the pier spacing is approximately 5–6 times the test pier diameter (D). Because the stand-alone dynamic rapid pier load test (PLT) requires no reaction pile to perform the test, it is assumed that the spacing requirement can be less stringent than that required by a static load test, even though no regulation regarding the spacing of test piers exists. Additionally, our FEM analysis (Wang and Sitar 2011) shows that soil movement is primarily concentrated within a distance of 1D away from the test pier, and very little pier-to-pier interaction occurs if the spacing is approximately 5D. Therefore, the spacing of the piers' setup was considered to be adequate.

Conventional flight augers were used to drill the pier holes, and concrete was placed in each hole on the day of drilling. Compressible material was placed beneath all 61-cm (2-ft)-diameter piers to ensure that the test load was predominantly transferred through side friction. Pier A1-19, on the other hand, was installed with downhole cleaning to ensure good end bearing. Finally, an annular space was created around the upper 30 cm (1 ft) of each drilled pier to isolate any possible resistance contribution from the concrete pavement section to the axial capacity of the drilled piers.

The load test program commenced after a curing period of 18 days. Three types of tests were performed. First, PLTs were performed on all six test piers to obtain dynamic load-displacement information. Second, quick static-compression and tension tests were performed based on the ASTM D1143 and ASTM D3689 (ASTM 2007a, b). To evaluate the impact of the pier test sequence on the results, dynamic PLTs were performed again on some of the test piers to evaluate the differences in pier capacities and stiffness between the first and the second PLTs. A pier-by-pier summary of the test program is listed in Table 1.

The Fundex PLT is designed to produce long-lasting blows on the pier head. Fig. 5 shows field photos from the test setup. To conduct a PLT, a 25-metric-ton mass is hydraulically lifted by a mobile

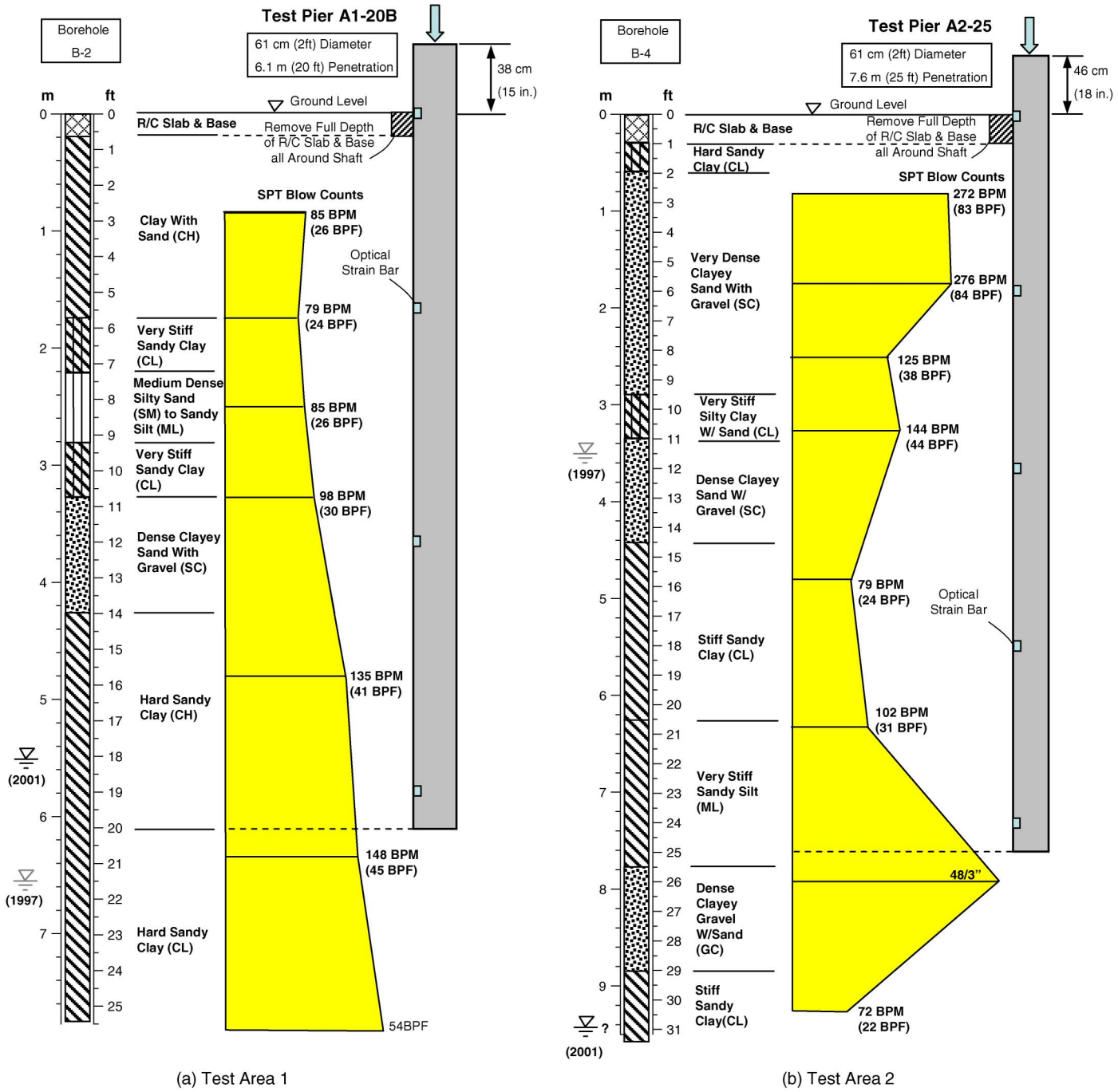

Fig. 2. Soil profiles with examples of test pier layout

track-mounted rig to a predetermined height to create the potential energy. The mass is then released and free-falls onto a striker plate. Large damping springs spread the impact load over a period of approximately 200 milliseconds (ms). The hydraulic system catches the mass on the rebound to allow only one strike on the pier per drop. The resulting duration of load application reasonably simulates an effective period of earthquake loading, making the device a good predictor of pier behavior in seismic loading regardless of soil type (Schellingerhout and Revoort 1995). By raising the mass to successively larger drop heights, a family of individual load-displacement curves is produced and the corresponding residual displacements are recorded. The peaks of the individual load-displacement curves define a classic load-displacement curve for the test pier.

During the PLT, pier-head vertical displacements were recorded for each drop, using an optical diode transmitter fastened to the face of the test pier and recorded by a camera receiver 9 m away to minimize disturbance by vibration. The optical and electrical strain bars were installed at predetermined locations along the length of the drilled piers so that the contribution of each soil stratum to drilled-pier capacity could be isolated and quantified. Both of the optical strain bar and electrical strain bar readings were taken simultaneously at a frequency of 1 kHz.

It is worth comparing the PLT conducted in this test program with other methods of dynamic tests. For example, the nondestructive vibration test has been widely used in estimating the stiffness, length, and cross-sectional area of intact piles

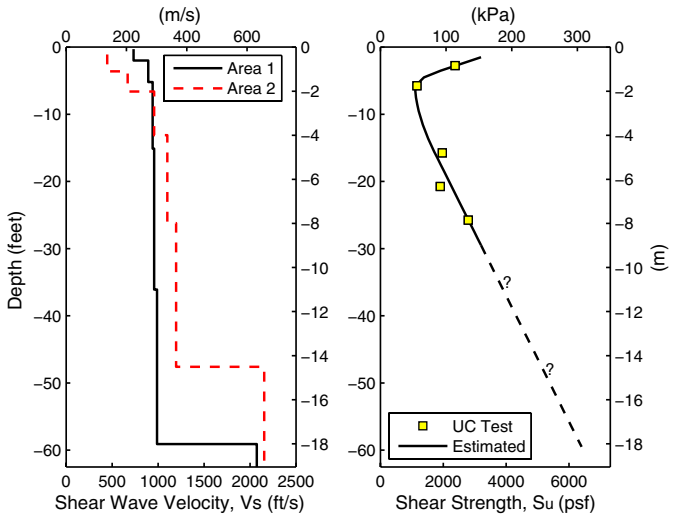

Fig. 3. Shear-wave velocity and shear-strength profile for Test Areas 1 and 2

(Davis and Robertson 1976). These vibration tests are designed to measure small-strain wave reflection within the test pile, and the amplitude of impact during the test is only tens of kPa, with the duration and pile-head displacement on the order of several milliseconds and 10^{-9} to 10^{-7} m, respectively. On the other hand, the PLT is quite similar to the STATNamic pile load test (see Middendorp et al. 1992; Paikowsky 2006) in some aspects. The STATNamic test uses high gas pressure generated by burning of fuel inside the device to exert short-duration (on the order of 100 ms) load on the pile. The STATNamic test therefore usually fully mobilizes the soil resistance in a single load cycle, and the test has been primarily used to determine equivalent static pile capacity. Because the main objective of this paper is to explore the dynamic stiffness, dynamic capacity, and the energy-dissipation characteristics of the pier-soil system from the PLT, it is beyond the scope of the work to compare various analytical methods that were developed to derive the static capacity of the pier from the dynamic tests.

Test Results

Loading Rate Effects

The PLT on Pier A1-19 consisted of a series of nine consecutive blows, which progressively loaded the pier from a small-strain level to the yield state, with increasing magnitudes of impact load. The PLT axial load versus the pier-head displacement curves are shown in Fig. 6(a), and a dynamic load-displacement envelope is defined to encompass all loading cycles. To examine the effects of loading rate on Pier A1-19, the PLT was followed by a static-compression test using a reaction beam and the adjacent flank Piers A1-20A and A1-20B. The heavy solid line in Fig. 6(a) shows the static load-displacement curve, which starts from approximately 1.3 cm (0.5 in.) of residual displacement that resulted from the PLT. To make comparison of the response for each load increment easier, each PLT loop and the static curve are replotted from the same origin in Fig. 6(b).

Clearly, the dynamic and the static stiffnesses of the pier-soil system depend on the applied load or displacement level. The small-strain elastic stiffness of the pier-soil system can be approximated by an elastic solution proposed by Randolph and Wroth (1978). In this solution, the elastic stiffness of the soil-pier system, K_{max}, depends on small-strain soil modulus and the pier configuration.

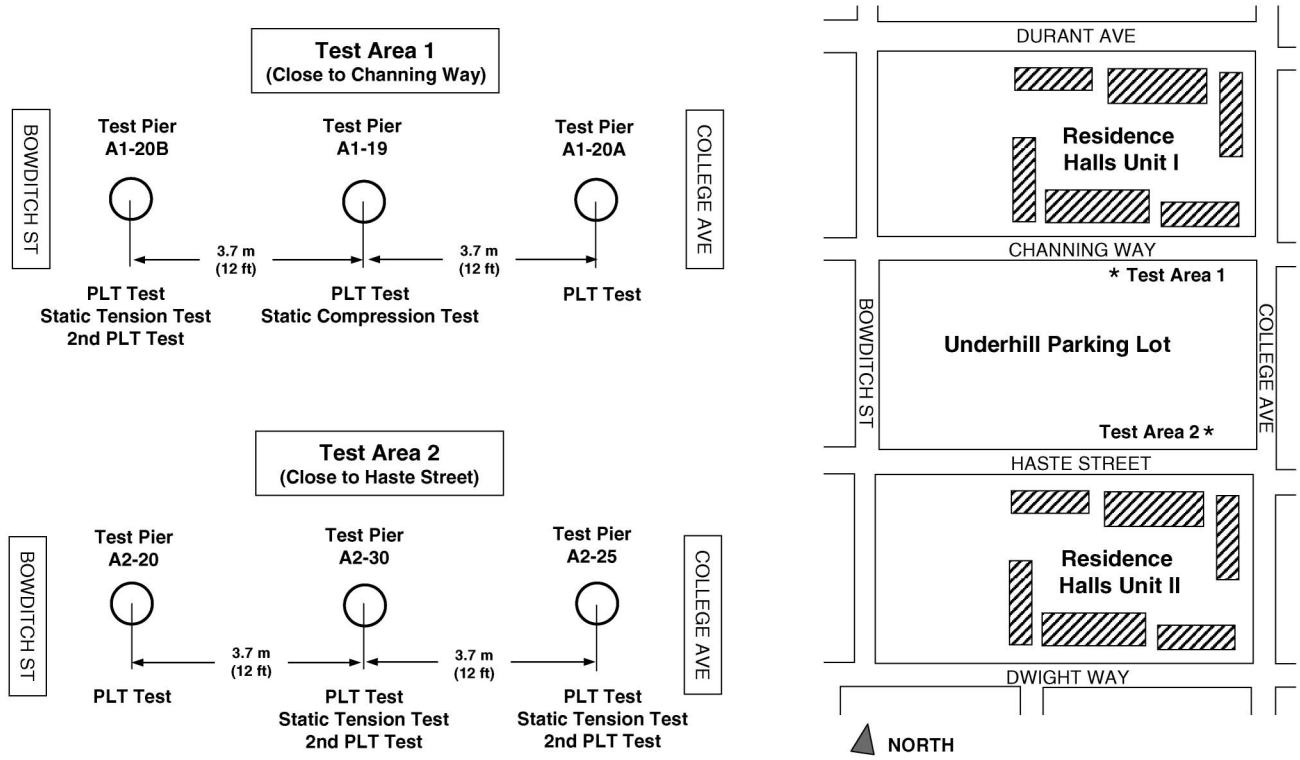

Fig. 4. Arrangement of test piers

Table 1. Summary of Testing Program on Drilled Shafts

Test Area 1			Test Area 2		
A1-20B [$D = 61$ cm (2 ft); $L = 6.1$ m (20 ft)]	A1-19 [$D = 76$ cm (2.5 ft); $L = 5.8$ m (19 ft)]	A1-20A [$D = 61$ cm (2 ft); $L = 6.1$ m (20 ft)]	A2-20 [$D = 61$ cm (2 ft); $L = 6.1$ m (20 ft)]	A2-30 [$D = 61$ cm (2 ft); $L = 9.1$ m (30 ft)]	A2-25 [$D = 61$ cm (2 ft); $L = 7.6$ m (25 ft)]
First PLT (10-01-2001) Static tension (10-04-2001) Second PLT (10-04-2001)	PLT (10-02-2001) Static compression (10-03-2001)	PLT (10-02-2001)	PLT (10-03-2001)	First PLT (10-03-2001) Static tension (10-05-2001) Second PLT (10-05-2001)	First PLT (10-03-2001) Static tension (10-05-2001) Second PLT (10-05-2001)

Note: D = pier diameter; L = pier length.

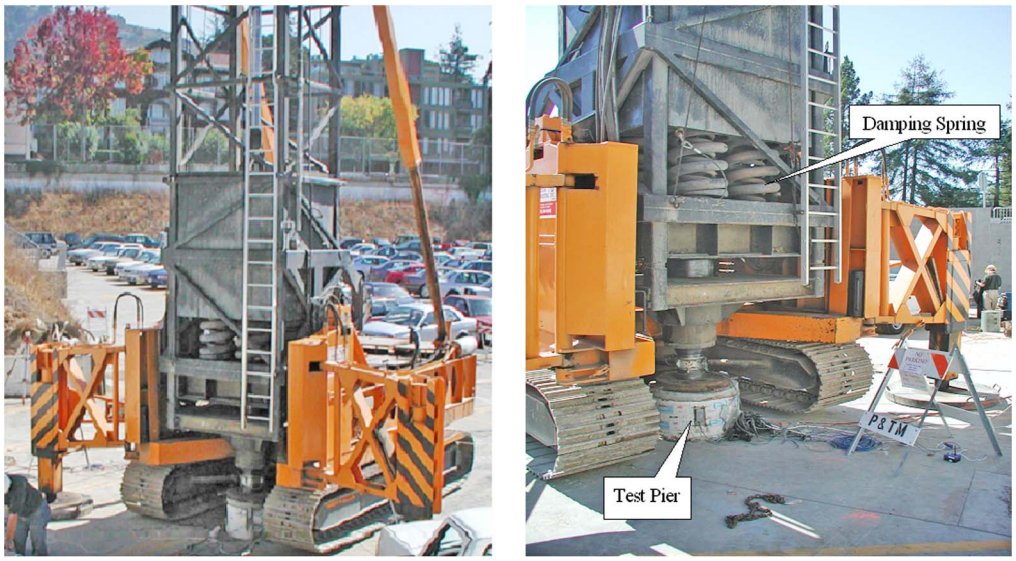

(a) Fundex PLT Rig (b) Close-up Loading Unit

Fig. 5. Rapid PLT using Fundex PLT equipment

$$K_{\max} = K_{\text{shaft}} + K_{\text{tip}} = \frac{2\pi G_{\max} L}{\ln(r_m/r_0)} + \frac{2G_{\max} D}{1-v} \tag{1}$$

where the first and the second term represent contributions of the shaft resistance and the tip resistance to the elastic stiffness, respectively; D = pier diameter; L = pier length; $r_m = 2.5L(1-v)$; and v = Poisson's ratio of the soil (chosen as 0.4 if the soil is unsaturated). The small-strain shear modulus of the soil, $G_{\max}$, can be estimated through the well-known relationship $G_{\max} = \rho V_s^2$, where ρ = density of the soil and V_s = shear-wave velocity of the site. Using parameters from the site investigation, the elastic stiffness of Pier A1-19 was estimated as $K_{\max} = 2.37 \times 10^6$ kN/m.

Stiffness reduction of the soil-pier system with respect to the displacement level is an important property in seismic design. Fig. 7(a) plots the stiffness ratio η (defined as the secant stiffness normalized by the elastic stiffness $K_{\max}$) versus displacement ratio (vertical pier-head displacement normalized by pier radius) for Pier A1-19. Similar to the well-known modulus degradation curves of soils, the stiffness ratios of dynamic and static response degrade with increasing displacement levels. The system stiffness approaches the elastic solution $K_{\max}$ when the displacement ratio is less than 0.1% of pier radius. The secant stiffness degrades to 15–25% of $K_{\max}$ where the displacement ratio is approximately 1–2%. Because of the rate effect, the dynamic stiffness ratio is approximately 20–40% greater than that of the static curve at almost all displacement levels. Correspondingly, the dynamic capacity is approximately 30% greater than the static capacity based on the Davisson offset limit method (Davisson 1972). The test results corroborate the notion that the axial pier capacity can significantly increase with loading rate. Audibert and Dover (1982) have compiled field pile load tests at varying loading rates conducted at different clay sites. Although a large amount of scatter was noted in their data, the ratio of ultimate dynamic capacity to the static capacity shows a definite trend with increased loading rate. In the range of loading rates corresponding to wave and earthquake loading, they found the ultimate axial capacity of a pier increases by 20–80%.

Energy Dissipation

The hysteretic energy-dissipation characteristics of the soil-pier system, defined as the area enclosed by each cyclic force-displacement loop, are calculated and plotted in Fig. 7(b). The energy-dissipation curve also depends on the displacement level, similar to that of the soils. The displacement-dependent stiffness ratio and energy-dissipation characteristics derived from the PLT can be used directly to quantify the dynamic properties of the soil-pier system in seismic design.

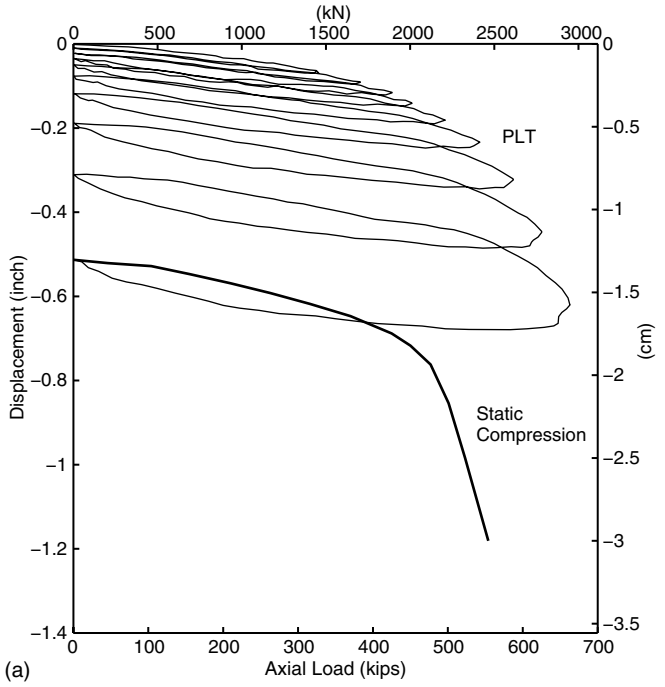

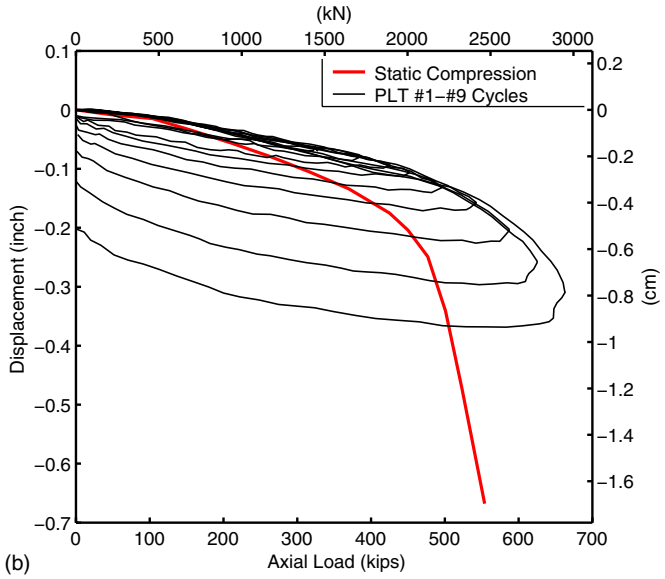

Fig. 6. Load-displacement curves for PLT and static-compression test on Pier A1-19

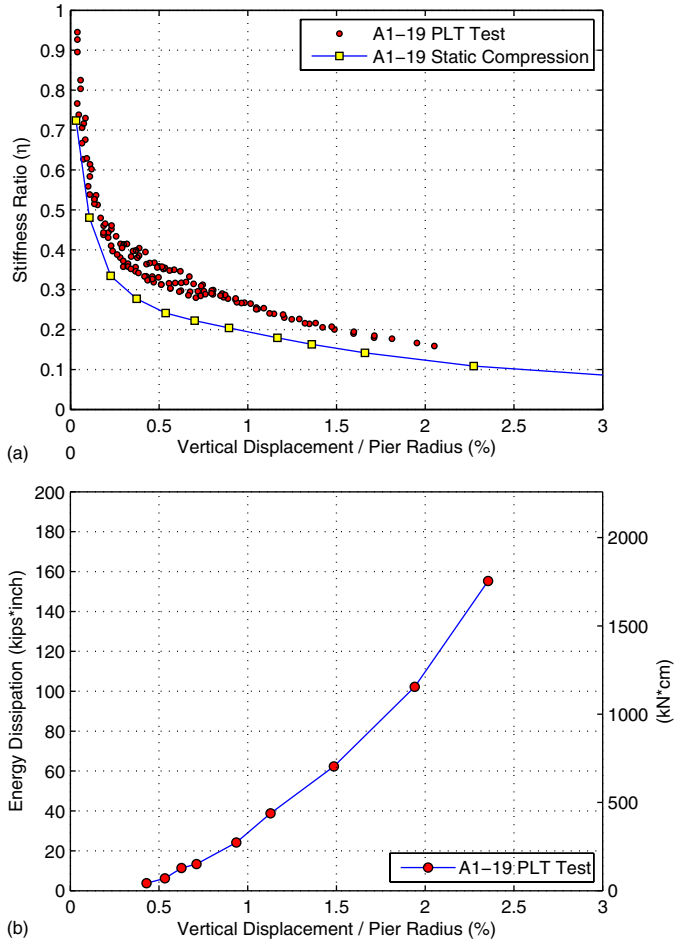

Fig. 7. Stiffness ratio and energy-dissipation characteristics of Pier A1-19

Fig. 8(a) shows the PLT results for Pier A1-20A loaded by 10 consecutive load cycles. Each PLT loop is replotted from the same origin in Fig. 8(b) for comparison. The energy dissipation against the residual displacement for each load cycle from Piers A1-19 and A1-20A tests shows an approximately linear relationship in Fig. 9(a), implying that the energy is primarily dissipated to overcome a constant resistance. The slope of the straight line fit, F, can therefore be interpreted as the effective resistance force of the pier-soil system. The effective resistance force F was found to be 3,492 kN (785 kips) for Pier A1-19, and 2,184 kN (491 kips) for Pier A1-20A. Systematic evaluation of the effective resistance force for all piers is provided subsequently.

The peak load versus the residual displacement in Fig. 9(b) shows a significant increase in the residual displacement once the peak load exceeds a certain limit. There exists an elastic threshold load, below which very little residual displacement could accumulate, making the pier behavior virtually elastic. In this paper, the elastic threshold load is defined as corresponding to the peak load with a residual displacement of 0.1% pier radius. By examining the results, the elastic threshold accounted for approximately 40–70% of the dynamic capacity determined from the Davisson offset limit method, which implies that a factor of safety of 2–2.5 is adequate to limit the residual displacement in dynamic design.

Cyclic Degradation

In general, cyclic loads tend to counteract rate effects so that capacity and stiffness degrade with repeated loading cycles. The effect of cyclic loading on the ultimate pier capacity seems at first glance to be quite contrary to the observed behavior in cyclic pile load tests. On the one hand, large cyclic capacity degradation was previously observed under cyclic displacement-controlled tests (Grosch and Reese 1980); on the other hand, the ultimate axial capacity was reported to be only slightly (10–15%) affected under one-way cyclic load-controlled tests. Kraft et al. (1981) reported that the pier capacity after cyclic loading exceeded its static capacity (i.e., no apparent reduction of ultimate static capacity after the cyclic load test). They suggested that "the total effects of the loading history must be evaluated together with loading rate." Therefore, the two different forms of cyclic load tests must be distinguished. One-way cyclic tests impose cyclic loading without reversal of the load (e.g., compression only, as in the PLT), whereas the loading in two-way cyclic tests produces a complete reversal of load. Complete

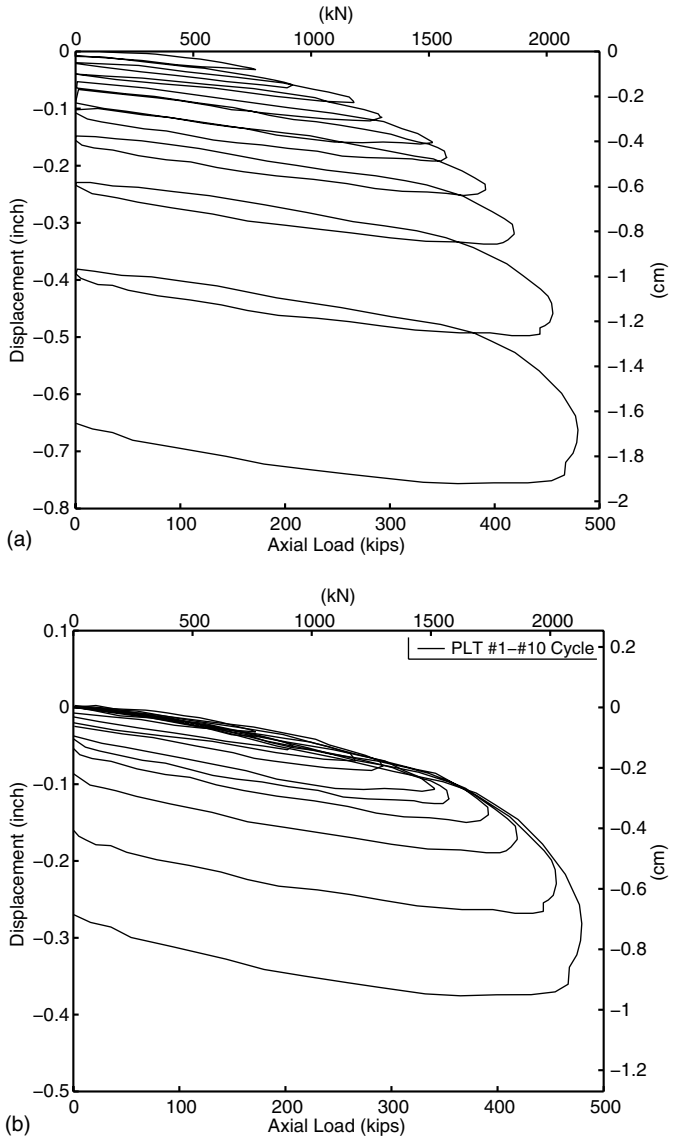

Fig. 8. Load-displacement curves for PLT on Pier A1-20A

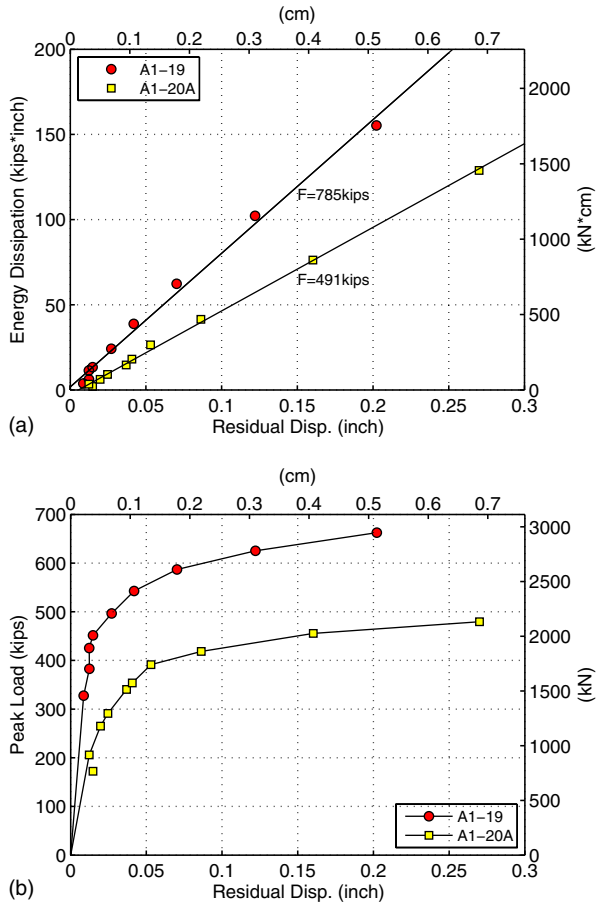

Fig. 9. Energy dissipation and peak load versus residual displacement of Piers A1-19 and A1-20A

stress reversal in a two-way cyclic test induces much more severe structural damage in the soil owing to remolding along the piers and at the tip, causing more rapid and severe pier loading capacity and stiffness degradation than the one-way cyclic test.

To examine the effect of stress reversal on the subsequent performance of a single pier, a sequence of load tests was designed for Pier A1-20B as follows. First, the PLT was performed on Pier A1-20B. After the PLT, the pier was subjected to a static-tension test, and a second PLT was performed. Fig. 10 summarizes the recorded pier-head displacement and the applied axial load for all tests performed on Pier A1-20B.

The static-tension capacity of the test pier after the PLT was approximately 2/3 of the dynamic capacity, all determined from Davisson offset limit method. The difference can be partially attributed to the different loading rate of these two tests and the influence of the preceding cyclic PLT compression. The effects of cyclic degradation were exhibited in significant stiffness and capacity degradation in the second PLT, in which the dynamic capacity was only approximately 50% of that in the first PLT. This finding suggests that a full stress reversal during earthquake loading can lead to significant degradation of the pier capacity and is consistent with soil behavior previously documented under cyclic loading.

Fig. 11 compares the energy dissipation and the peak load versus the residual displacement of the first and the second PLTs. Again, a linear relationship can be found between energy dissipation and the residual displacement for both PLTs. F was reduced from 1,633 kN (367 kips) in the first PLT to approximately 70%, i.e., 1,139 kN (256 kips) in the second PLT. Similarly, the elastic threshold in the second PLT [222 kN (50 kips)] was only approximately 1/3 of that of the first PLT [667 kN (150 kips)].

The effect of cyclic degradation was also measured on Pier A2-25. The PLT was followed by a static-tension test and a second PLT. A comparison of the load-displacement curves for the initial PLT and the static-tension test in Fig. 12 confirmed that the impact of the initial PLT on the subsequent static test was relatively small. However, a comparison of the two PLT curves in Fig. 12, in terms of the stiffness and capacity, again showed that the complete load reversal in the static-tension test substantially affected the pier response in the second PLT.

Although these tests represented a rather extreme condition of complete load reversal with uplift and did not address the condition of partial load reversal, they clearly show that such loading could severely reduce the dynamic stiffness and dynamic load capacity of pier foundations subjected to seismic loading.

Summary of Test Results

Table 2 summarizes F values derived from all PLTs. To allow for comparison between piers of different configurations, the

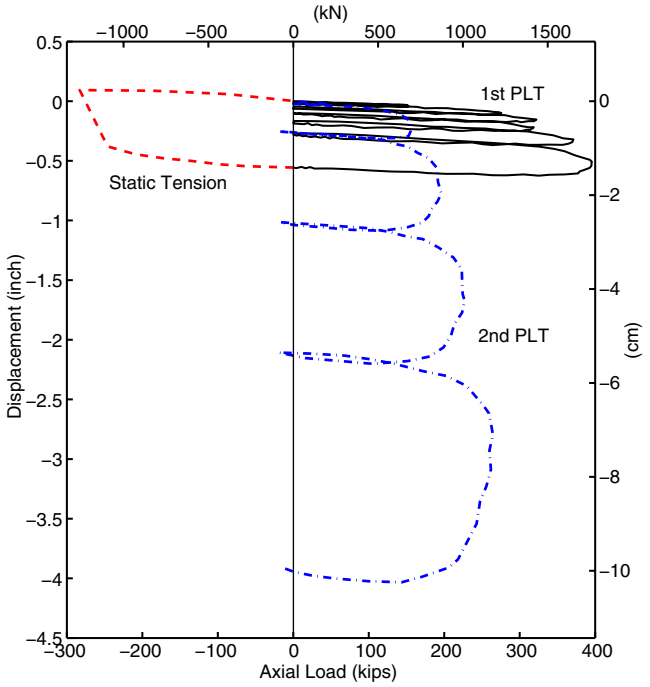

Fig. 10. Load-displacement plot for Pier A1-20B

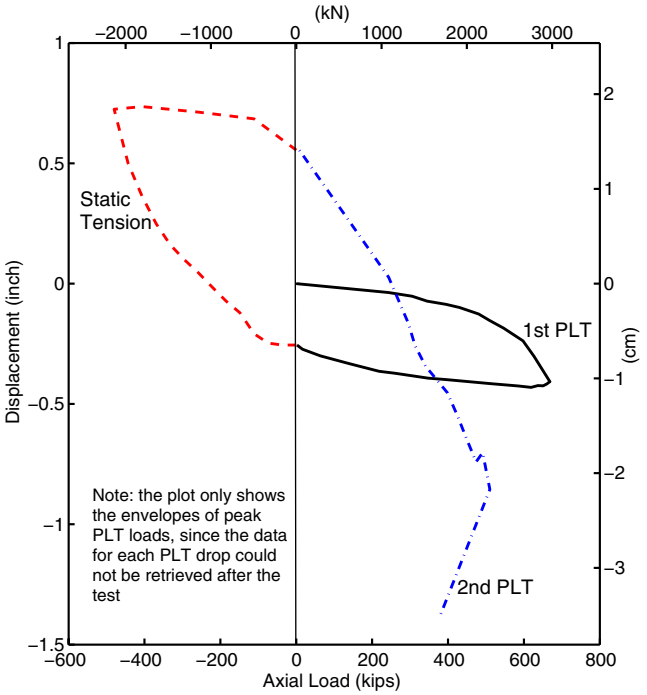

Fig. 12. Load-displacement plot for Pier A2-25

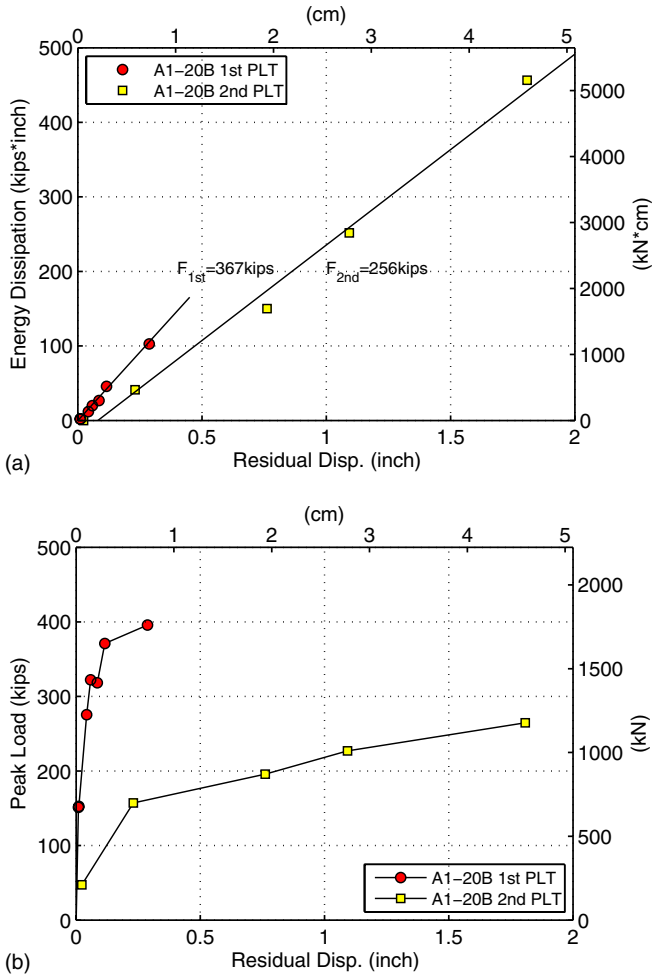

Fig. 11. Energy dissipation and peak load versus residual displacement of Pier A1-20B

Table 2. Summary of Effective Resistance Force F for PLTs

Pier	L m (ft)	D cm (ft)	F kN (kips)	$f = F/\pi DL$ kPa (kips/ft^2)
A1-19	5.8 (19)	76 (2.5)	3,487 (784)[a]	251 (5.25)[a]
A1-20A	6.1 (20)	61 (2.0)	2,184 (491)	187 (3.90)
A1-20B (first)	6.1 (20)	61 (2.0)	1,637 (368)	140 (2.92)
A1-20B (second)			1,139 (256)	98 (2.04)
A2-20	6.1 (20)	61 (2.0)	2,576 (579)	221 (4.61)
A2-25	7.6 (25)	61 (2.0)	3,670 (825)	252 (5.25)
A2-30	9.1 (30)	61 (2.0)	4,386 (986)	250 (5.23)

[a]Includes end-bearing resistance.

effective resistance per unit area, f, is also given in the table. In general, the effective resistance was in the range of approximately 100–120% of the dynamic capacity interpreted from the Davisson offset limit method in each test. Because the Davisson offset limit usually provides an overly conservative estimation of axial compressive capacity for cast-in-place piles, as pointed out by NeSmith and Siegel (2009), F may be used as an alternative criterion to evaluate the dynamic pier strength. The normalized effective resistance, f, is apparently related to the dynamic shear strength of the soils. At this moment, more field tests are still needed to develop a robust correlation.

To allow for better comparison of all results from the test program, the load-displacement curves are normalized, as shown in Figs. 13 and 14. The total pier resistance is divided by surface area of the pier to obtain an average unit shaft resistance. Because only Pier A1-30 has end-bearing resistance, that resistance has been subtracted from the total resistance before normalization. For clarity, only the cyclic envelopes for PLT results are plotted, with each data point representing the peak load in each cyclic loop.

As shown in Fig. 13, the normalized PLT curves virtually coincide for all piers in Test Area 1, except Pier A1-20B, which

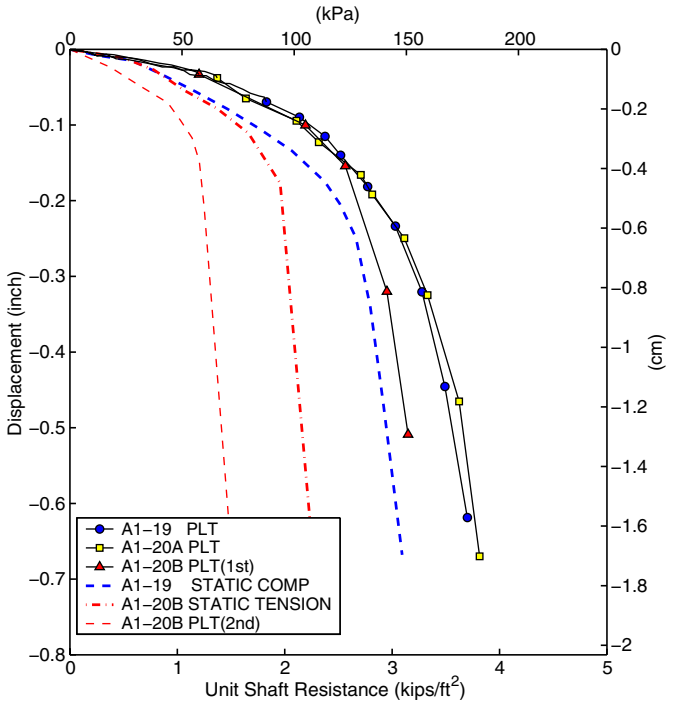

Fig. 13. Normalized pier load test results (Test Area 1)

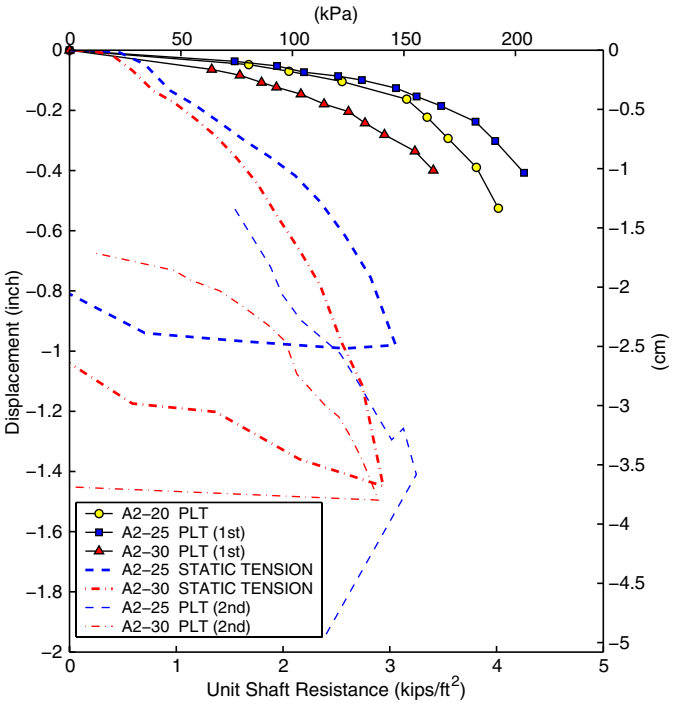

Fig. 14. Normalized pier load test results (Test Area 2)

Table 3. Mobilized Ultimate Pier Resistance per Unit Area (in kPa)

	PLT		Static test	
Test pier	First	Second	Compression	Tension
A1-19	171[a]		140[a]	
A1-20A	172			
A1-20B	149	70		100

[a]Frictional resistance only; assume the end-bearing takes 1/6 of the total resistance.

Table 4. Estimated Stiffness Ratio η for Pier-Soil System under Working Load

	PLT		Static test	
Test pier	First	Second	Compression	Tension
A1-19	0.3–0.4		0.2–0.3	
A1-20A				
A1-20B		0.15		0.2–0.3

Note: Working load is assumed as a half of the pier capacity determined by the Davisson offset limit method.

yields a lower ultimate resistance. The ultimate resistance determined from the Davisson offset limit method for each pier test is normalized by pier geometry in Table 3. The static-compression and static-tension curves have almost the same initial slope, but the mobilized ultimate resistance in tension is approximately 70% of the ultimate resistance in compression. The loading rate effect is evident when comparing the PLT results with the static-compression and static-tension tests. The PLTs showed that 20–40% greater ultimate resistance is mobilized in dynamic cases. Load reversal leads to a 50% reduction in both stiffness and ultimate resistance when comparing the second PLT to the first.

The estimated stiffness ratio η for the pier-soil system under working load is back-analyzed from field data. The working load is assumed to be half of the pier capacity determined by the Davisson offset limit method, implying a design factor of safety of 2. The results presented in Table 4 show that a modulus ratio between 0.3 and 0.4 can reasonably approximate the secant dynamic stiffness over the range of the working load. The stiffness ratio of the static compression and tension is around 0.2–0.3, while for the second PLT, the ratio decreases to 0.15 owing to stiffness degradation. The elastic stiffness estimated in Eq. (1) and the recommended stiffness ratios in Table 4 provide a simple means for estimating the secant stiffness of the pier foundation under the working load.

Conclusions

Prototype load tests on cast-in-place concrete piers were performed to examine dynamic and static responses of pier-soil systems under axial loading. In particular, loading rate effects, cyclic effects, and characteristics of hysteretic energy dissipation were evaluated from the field data. The test results showed that the dynamic capacity of the piers is 30% greater than the static resistance on the basis of the Davisson offset limit method, and the dynamic stiffness is approximately 20–40% greater than the static stiffness at almost all displacement levels. PLTs conducted on drilled piers subjected to full load reversal to failure in uplift also indicated that a pier might experience significant stiffness and strength degradation under similar loading, in which the stiffness and strength degradation can be more than 50%.

The preceding findings are limited to the in situ soil condition and piers tested. However, the test program showed that the PLT is a fast, innovative method to get useful site-specific information for seismic design of foundations. The case history presented in the paper shows the importance of collecting and analyzing relevant information, and the PLT can serve as a simple and easy technique to get a better handle on assessing the dynamic stiffness, capacity, and energy-dissipation characteristics of the piers. The subsequent use of the PLT results in the seismic design of the foundations for the new University of California, Berkeley Resident Units resulted in savings of approximately $400,000–$600,000 in foundation

costs (Moore et al. 2003) over the $125,000 cost of the test program. Additional savings were generated in the superstructure design, because higher foundation stiffness resulted in smaller rigid body motions in the superstructure and less dynamic displacements in general. Because the PLT is relatively fast and easy to perform, the test procedure is economical even for relatively small projects.

Acknowledgments

The PLT and static pier load tests were performed by American Piledriving, Inc. (API) of Pleasanton, California, under the direction of Rutherford and Chekene Consulting Engineers. Their cooperation and support are gratefully acknowledged. FISO Technologies of Canada fabricated the optical strain bars based on parameters provided by Lymon C. Reese and Associates, and the electrical strain bars were custom-built by Lymon C. Reese and Associates, which also monitored all the tests. An automated electronic data-acquisition system was provided on loan by FISO. The writers also appreciate the support and advice of Craig Comartin of Comartin Associates, the University of California, Berkeley, Capital Projects group, and FISO Technologies throughout the test program. The financial support for the test program was provided by University of California, Berkeley, Capital Projects, and the research was supported by Pacific Earthquake Engineering Research (PEER) Center under the National Science Foundation Award No. EEC-9701568. The first writer also acknowledges support from the University Grants Committee (UGC) of Hong Kong—Strategic Initiatives RPC11EG27, and the Li Foundation Heritage Prize. Finally, we thank anonymous reviewers for their helpful comments to improve the quality of the paper.

References

ASTM. (2007a). "Standard test methods for deep foundation under static axial compressive load." *D1143/D1143M-07*, West Conshohocken, PA.

ASTM. (2007b). "Standard test methods for deep foundations under static axial tensile load." *D3689-07*, West Conshohocken, PA.

Audibert, J. M. E., and Dover, A. R. (1982). "Discussion of "Pile load tests: Cyclic loads and varying load rates" by L. M. Kraft, E. A. Verner, and W. R. Cox." *J. Geotech. Engrg. Div.*, 108(3), 501–505.

Davis, A. G., and Robertson, S. A. (1976). "Vibration testing of piles." *J. Struct. Eng.*, 54(6), A7–A10.

Davisson, M. T. (1972). "High capacity piles." *Proc., Lecture Series on Innovations in Foundation Construction*, ASCE Illinois Section, Chicago, 81–112.

Grosch, J. J., and Reese, S. C. (1980). "Field tests of small-scale pile segments in a soft clay deposit under repeated axial loading." *Proc., 12th Offshore Technology Conf.*, American Institute of Mining, Metallurgical, and Petroleum Engineers (AIME), New York, 143–151.

Kraft, L. M., Cox, W. R., and Verner, E. A. (1981). "Pile load tests: Cyclic loads and varying load rates." *J. Geotech. Engrg. Div.*, 107(1), 1–19.

Middendorp, P., Berminghammer, P., and Kuiper, B. (1992). "STATNamic load testing of foundation piles." *Proc., 4th Int. Conf. of Applications of Stress-Wave Theory to Piles*, A. A. Balkema, Netherlands, 581–588.

Moore, K. S., Comartin, C. D., Kasali, G., and Lopez, W. A. (2003). "The benefits of physical testing: Two case studies at the University of California Berkeley." *Proc., SEAOC Convention*, Structural Engineers Association of California, Sacramento, CA.

NeSmith, W. M., and Siegel, T. C. (2009). "Shortcomings of the Davisson offset limit applied to axial compressive load tests on cast-in-place piles." *Contemporary Topics in Deep Foundations: Proc., Selected Papers of the 2009 Int. Foundation Congress and Equipment Expo*, ASCE, Reston, VA, 568–574.

Paikowsky, S. G. (2006). "Innovative load testing systems." *Rep. NCHRP 21-08*, National Cooperative Highway Research Program, Washington, DC.

Randolph, M. F., and Wroth, C. P. (1978). "Analysis of deformation of vertically loaded piles." *J. Geotech. Engrg. Div.*, 104(GT12), 1465–1488.

Schellingerhout, A. J. G., and Revoort, E. (1995). *The pseudo static load tester*, IFCO and Fundex BV, Netherlands.

Wang, G., and Sitar, N. (2011). "Static and dynamic axial response of drilled piers. II: Numerical simulation." *J. Geotech. Geoenviron. Eng.*, 137(12), 1143–1153.